

Phase diagrams, quantum correlations and critical phenomena of antiferromagnetic Heisenberg model on diamond-type hierarchical lattices

Pan-Pan Zhang¹, Zhong-Yang Gao², Yu-Liang Xu¹, Chun-Yang Wang¹ and Xiang-Mu Kong^{1,2*}

¹*School of Physics and Optoelectronic Engineering, Ludong University, Yantai 264025, China*

²*College of physics and Engineering, Qufu Normal University, Qufu 273165, China*

(Dated: July 13, 2021)

Abstract

The spin-1/2 antiferromagnetic Heisenberg systems are studied on three typical diamond-type hierarchical lattices (systems A, B and C) with fractal dimensions 1.63, 2 and 2.58, respectively, and the phase diagrams, critical phenomena and quantum correlations are calculated by a combination of the equivalent transformation and real-space renormalization group methods. We find that there exist a reentrant behavior for system A and a finite temperature transition in the isotropic Heisenberg limit for system C (not for system B). Unlike the ferromagnetic case, the Néel temperatures of antiferromagnetic systems A and B are inversely proportional to $\ln(\Delta_c - \Delta)$ (when $\Delta \rightarrow \Delta_c$) and $\ln \Delta$ (when $\Delta \rightarrow 0$), respectively. And we also find that there is a turning point of quantum correlation in the isotropic Heisenberg limit $\Delta = 0$ where there is a "peak" of the contour and no matter how large the size of system is, quantum correlation will change to zero in the Ising limit for the three systems. The quantum correlation decreases with the increase of lattice size L and it is almost zero when $L \geq 30$ for system A, and for systems B and C, they still exist when L is larger than that of system A. Moreover, as an example, we discuss the error of result in system A, which is induced by the noncommutativity.

PACS numbers:

*Corresponding author. E-mail address: kongxm668@163.com (X.-M. Kong).

I. INTRODUCTION

Fractals, due to their unique self-similar structure, have been widely studied theoretically and experimentally in physics and materials science over the past few decades, especially in the field of phase transitions and critical phenomena of spin systems[1, 2]. For classical spin systems on fractals, in particular, using the renormalization group (RG) method to study critical phenomena, there have been many conclusive results[1, 3, 4]. For quantum ferromagnetic spin systems on fractals, there are also some studies and conclusions, e.g., the research shows that the critical temperature $T_c = 0$ and $T_c > 0$ for the isotropic ferromagnetic Heisenberg system on diamond-type hierarchical (DH) lattice with fractal dimensions $d_f = 2$ and $d_f = 3$, respectively[5–7].

Relatively speaking, the calculation of antiferromagnetic (AF) system is more difficult than the ferromagnetic one. In recent years, various renormalization group approaches[8–11], Green’s function technique[12, 13], spin-wave theory [14] and Monte Carlo method [15, 16] have been applied to study the quantum AF Heisenberg systems on translationally symmetric lattices. Sousa et al. calculated the phase diagrams of the AF Heisenberg model by the mean-field RG approach and found that the AF Néel temperature $T_N < T_c$ and $T_N > T_c$ for two-dimensional (2D) and three-dimensional (3D) lattices, respectively[11, 17, 18]. However, results from spin-wave theory and Green’s function technique obtained $T_N = T_c$ for AF Heisenberg systems on 2D and 3D lattices [13, 14, 19]. Quantum Monte Carlo results indicate that an ordered low temperature phase is obtained even at much smaller anisotropies $\Delta \sim 10^{-3}$ for AF Heisenberg systems on 2D lattices [15, 20]. But there have been no reports of the study on AF spin systems on fractal lattices so far.

On the other hand, as an important quantum resource, quantum correlation has been applied to quantum communication, quantum teleportation and quantum computation, etc[21, 22]. Quantum correlation contains more quantum information than quantum entanglement which is a particular quantum correlation[23, 24]. The quantum discord (QD) which captures nonclassical correlation even without entanglement is proved as an effective measure for all aspects of quantum correlation[25, 26]. As a wider class of measures than entanglement, QD has become an active research topic over the past few years[27–30], which has important application in quantum information processing, quantum dynamics and even biophysics[31–34]. But, it isn’t difficult to find that the present studies have focused on the

one-dimensional spin chain, the studies of fractal lattices are less[28, 35]. It is significant to study the quantum correlation of fractal lattice systems, which is helpful to understand the influence of fractal structure on quantum information.

In this work, we investigate the phase diagrams, critical phenomena and QDs of the AF Heisenberg model on three kinds of DH lattices (systems A, B and C) with fractal dimensions $d_f = 1.63, 2$ and 2.58 , respectively, which is shown in Fig. 1. Using the real-space RG method straightforwardly, we study system A and obtain the relations between quantum correlation with temperature and the anisotropic parameter. For systems B and C, we apply a combination of the equivalent transformation and real-space RG methods. On this basis, we hope to explore the relatively universal laws through the further study of the fractal lattice systems.

The structure of this manuscript is organized as follows. In Sec. II we summarize the method and study the phase diagram and critical behavior of system A. In Sec. III the method and the results are presented for systems B and C. Sec. IV discusses the quantum correlations of the three systems. In Sec. V the quantum effect and error of result are discussed. The summary is given in the last section.

II. THE METHOD AND CRITICAL BEHAVIORS OF SYSTEM A

The spin-1/2 Heisenberg model is described by the effective Hamiltonian

$$H = K \sum_{\langle ij \rangle} [(1 - \Delta)(\sigma_i^x \sigma_j^x + \sigma_i^y \sigma_j^y) + \sigma_i^z \sigma_j^z], \quad (1)$$

where $K = J/k_B T$, J is the exchange coupling constant ($J > 0$ and $J < 0$ correspond to ferromagnetic model and AF one, respectively), k_B the Boltzmann constant, T the temperature, $\langle ij \rangle$ denotes nearest-neighbor sites of this system, Δ is the anisotropic parameter, and σ_i^α ($\alpha = x, y, z$) are Pauli operators at site i . Note that, as particular cases, the Hamiltonian describes the Ising ($\Delta = 1$), isotropic Heisenberg ($\Delta = 0$) and XY ($\Delta = -\infty$) models, respectively.

In this section, we study the phase diagram and critical behavior of system A by the real-space RG method[36, 37]. Such kind of lattice is constructed in an iterative manner which can be realized by continuously replacing the dimer (a two-sites) with the generator[38] (Fig. 1). The RG transformation process system A is shown in Fig. 2(a).

As we can see, after summation of the internal spins, the generator (Fig. 2(a1)) is transformed into a new structure — a dimer (Fig. 2(a2)), which contains σ_1 and σ_2 . This procedure can be described as

$$\exp(H'_{12}) = \text{Tr}_{3456} \exp(H_{123456}), \quad (2)$$

where

$$H'_{12} = K'[(1 - \Delta')(\sigma_1^x \sigma_2^x + \sigma_1^y \sigma_2^y) + \sigma_1^z \sigma_2^z] + K_0$$

and

$$\begin{aligned} H_{123456} = & K(1 - \Delta)[(\sigma_1^x \sigma_3^x + \sigma_1^y \sigma_3^y) + (\sigma_1^x \sigma_6^x + \sigma_1^y \sigma_6^y) + (\sigma_3^x \sigma_4^x + \sigma_3^y \sigma_4^y) \\ & + (\sigma_5^x \sigma_6^x + \sigma_5^y \sigma_6^y) + (\sigma_2^x \sigma_5^x + \sigma_2^y \sigma_5^y) + (\sigma_2^x \sigma_4^x + \sigma_2^y \sigma_4^y)] \\ & + K(\sigma_1^z \sigma_3^z + \sigma_1^z \sigma_6^z + \sigma_3^z \sigma_4^z + \sigma_5^z \sigma_6^z + \sigma_2^z \sigma_5^z + \sigma_2^z \sigma_4^z) \end{aligned}$$

are the Hamiltonians of the renormalized dimer and of the generator, respectively. Tr_{3456} denotes a partial trace over the internal $\sigma_i (i = 3, 4, 5, 6)$. To make Eq. (2) possible, an additional constant K_0 has been included in H'_{12} . The RG recursion relations between the renormalized (Δ', K') and the original (Δ, K) parameters are determined by Eq. (2). Notice that the noncommutativity between the Hamiltonians of the neighboring generators is neglected, therefore the results are approximations which will be discussed in Sec. V.

In order to calculate the partial trace in Eq. (2), we expand $\exp(H'_{12})$ as

$$\exp(H'_{12}) = a' + b'_{12}(\sigma_1^x \sigma_2^x + \sigma_1^y \sigma_2^y) + c'_{12} \sigma_1^z \sigma_2^z, \quad (3)$$

where a' , b'_{12} and c'_{12} are functions of Δ' , K' and K_0 . In the direct product representation of σ_1^z and σ_2^z , both the left-hand side and right-hand side of Eq. (3) can be expressed as 4×4 matrixes and we finally obtain

$$\exp(4K') = \frac{(a' + c'_{12})^2}{(a' - c'_{12})^2 - 16b'^2_{12}}, \quad (4)$$

$$\exp(4\Delta'K') = \frac{(a' + c'_{12})^2}{(a' + 4b'_{12} - c'_{12})^2}, \quad (5)$$

$$\exp(K_0) = \frac{a' + c'_{12}}{\exp(K')}. \quad (6)$$

Similarly, we expand $\exp(H_{123456})$ as

$$\begin{aligned} \exp(H_{123456}) = & a + \sum_{\langle ij \rangle} [b_{ij} (\sigma_i^x \sigma_j^x + \sigma_i^y \sigma_j^y) + c_{ij} \sigma_i^z \sigma_j^z] \\ & + \sum_{\langle ij \rangle \neq \langle kl \rangle} A_{ij,kl} + \sum_{\langle ij \rangle \neq \langle kl \rangle \neq \langle mn \rangle} B_{ij,kl,mn} + r \sigma_1^z \sigma_2^z \sigma_3^z \sigma_4^z \sigma_5^z \sigma_6^z, \end{aligned} \quad (7)$$

in which

$$A_{ij,kl} = e_{ij,kl} (\sigma_i^x \sigma_j^x + \sigma_i^y \sigma_j^y) (\sigma_k^x \sigma_l^x + \sigma_k^y \sigma_l^y) + d_{ij,kl} (\sigma_i^x \sigma_j^x + \sigma_i^y \sigma_j^y) \sigma_k^z \sigma_l^z + f_{ij,kl} \sigma_i^z \sigma_j^z \sigma_k^z \sigma_l^z$$

and

$$\begin{aligned} B_{ij,kl,mn} = & g_{ij,kl,mn} (\sigma_i^x \sigma_j^x + \sigma_i^y \sigma_j^y) \sigma_k^z \sigma_l^z \sigma_m^z \sigma_n^z + p_{ij,kl,mn} (\sigma_i^x \sigma_j^x + \sigma_i^y \sigma_j^y) (\sigma_k^x \sigma_l^x + \sigma_k^y \sigma_l^y) \sigma_m^z \sigma_n^z \\ & + q_{ij,kl,mn} (\sigma_i^x \sigma_j^x + \sigma_i^y \sigma_j^y) (\sigma_k^x \sigma_l^x + \sigma_k^y \sigma_l^y) (\sigma_m^x \sigma_n^x + \sigma_m^y \sigma_n^y), \end{aligned}$$

where a , $\{b_{ij}\}$, $\{c_{ij}\}$, \dots $\{q_{ij,kl,mn}\}$ and r depend on K and Δ . From Eqs. (2), (3) and (7), it can be obtained that $a' = 16a$, $b'_{12} = 16b_{12}$, and $c'_{12} = 16c_{12}$, and the recursion relations become

$$\exp(4K') = \frac{(a + c_{12})^2}{(a - c_{12})^2 - 4b_{12}^2}, \quad (8)$$

$$\exp(4\Delta'K') = \frac{(a + c_{12})^2}{(a + 2b_{12} - c_{12})^2}. \quad (9)$$

By numerically iterating Eqs. (8) and (9), the AF phase diagram is obtained, which is shown in Fig. 3. There are two stable fixed points at $(1, \infty)$ and $(1, 0)$ and two unstable fixed points at $(1, 0.94)$ and $(0, 0)$, which corresponding to the Ising and the isotropic Heisenberg models, respectively. For comparison, the inset shows the critical line of the ferromagnetic system. We can see that there exists two phases in AF system, namely, the ordered and disordered phases, respectively. The Ising fixed point of the ferromagnetic system is the same as that of the AF one. At the Ising fixed point, we obtain the correlation length critical exponent

$$\nu = \frac{\ln b}{\ln \lambda} = 1.779, \quad (10)$$

where $b = 3$ is the scaling factor and $\lambda \equiv (\partial K' / \partial K) |_{\Delta=1, k_B T / |J|=0.94}$. At the isotropic Heisenberg fixed point of the ferromagnetic model, we obtain $\nu = 0$. For the AF model, the phase diagram is different from the ferromagnetic one: the critical line goes to zero at $\Delta_c = 0.703$ (quantum critical point). Moreover, we find a reentrant behavior in the phase

diagram. This fact is usually due to the quantum fluctuation which is related to the critical temperature and the anisotropy parameter and we will discuss it in Sec. V. Furthermore, we also study the critical temperature of this system when $T \rightarrow 0$. As shown in Fig. 4, for the ferromagnetic case the curie temperature satisfies

$$T_c \sim \Delta \quad (11)$$

and for the AF case the Néel temperature T_N satisfies

$$T_N \sim \frac{1}{\ln(\Delta_c - \Delta)}, \quad (12)$$

where $\Delta_c = 0.703$.

III. THE METHOD AND THE RESULTS FOR SYSTEMS B AND C

In this section, we use an effective combination of the equivalent transformation and real-space RG methods to study the AF Heisenberg model on systems B and C, which has been used for classical systems in Ref. [38] but for quantum systems this is done for the first time as far as we know. As we can see, antiferromagnetic interactions ($K < 0$) change to ferromagnetic interactions ($K' > 0$) by the ET is shown in Fig. 2(b). Therefore, we can obtain the critical point of an AF system if we know that of the equivalent system with ferromagnetic couplings. This method contains two steps (see Fig. 2(b)): (1) The ET technique is used to transform the AF system into an equivalent ferromagnetic one and the equivalent transformation equations are obtained. (2) By numerically iterating the RG recursion equations of the equivalent ferromagnetic system can be obtained. The results obtained from the second step are substituted into the ET equations in the first step and the AF phase diagram can be obtained.

In the following, we give the calculation procedure of the AF Heisenberg model for system B. To construct the equivalent transformation equations, we transform the cluster of Fig. 2(b1) (which contains four $\sigma_i (i = 1, 2, 3, 4)$) into Fig. 2(b2) (the cluster contains two spins 1 and 2). Following the same steps as in Sec. II, we can obtain the ET equations in

the same form as Eqs. (4)–(6), as well as the 16×16 matrix

$$\begin{aligned}
\exp(H_{1234}) &= a + \sum_{\langle ij \rangle} [b_{ij}(\sigma_i^x \sigma_j^x + \sigma_i^y \sigma_j^y) + c_{ij} \sigma_i^z \sigma_j^z] \\
&+ \sum_{\langle ij \rangle \neq \langle kl \rangle} d_{ij,kl} (\sigma_i^x \sigma_j^x + \sigma_i^y \sigma_j^y) \sigma_k^z \sigma_l^z \\
&+ \sum_{\langle ij \rangle \neq \langle kl \rangle} e_{ij,kl} (\sigma_i^x \sigma_j^x + \sigma_i^y \sigma_j^y) (\sigma_k^x \sigma_l^x + \sigma_k^y \sigma_l^y) \\
&+ f \sigma_1^z \sigma_2^z \sigma_3^z \sigma_4^z,
\end{aligned} \tag{13}$$

where a , $\{b_{ij}\}$, $\{c_{ij}\}$, $\{d_{ij,kl}\}$, $\{e_{ij,kl}\}$ and f are functions of K and Δ . Then using some similar calculations, it is obtained that $a' = 4a$, $b'_{12} = 4b_{12}$ and $c'_{12} = 4c_{12}$, and we finally obtain the equivalent transformation equations as

$$\exp(4K') = \frac{(a + c_{12})^2}{(a - c_{12})^2 - 4b_{12}^2}, \tag{14}$$

$$\exp(4K' \Delta') = \frac{(a + c_{12})^2}{(a + 2b_{12} - c_{12})^2}, \tag{15}$$

in which a , b_{12} , c_{12} are functions of K and Δ and the equivalent system has ferromagnetic interactions $K' > 0$. For the equivalent ferromagnetic system, we obtain the RG recursion relations in the same form as Eqs. (14) and (15)

$$\exp(4K'') = \frac{(a + c_{12})^2}{(a - c_{12})^2 - 4b_{12}^2}, \tag{16}$$

$$\exp(4K'' \Delta'') = \frac{(a + c_{12})^2}{(a + 2b_{12} - c_{12})^2}, \tag{17}$$

where a , b_{12} , c_{12} are functions of K' and Δ' . Then, we substitute K' and Δ' which are obtained by numerically iterating the ferromagnetic RG equations (16) and (17) into Eqs. (14) and (15), and finally get the phase diagram of the AF system.

Using the same procedure, we calculate the phase diagram of system C. However, the analytical expressions of the right-hand side in Eqs. (14) and (15) are difficult to calculate. In order to get the expressions, we expand $\exp(H_{12345})$ approximately as

$$\exp(H_{12345}) \approx 1 + H_{12345} + \frac{H_{12345}^2}{2!} + \dots + \frac{H_{12345}^{11}}{11!}, \tag{18}$$

in which we adopt the first twelve terms for convenient calculation.

Fig. 5 shows the phase diagrams of systems B and C in $(\Delta, k_B T/|J|)$ space. The AF critical line of system A is also provided for comparison. There are two unstable fixed points

for system B at (1, 1.64) and (0, 0) (for system C at (1, 2.77) and (0, 2.06)), corresponding to the Ising and the isotropic Heisenberg fixed points, respectively. From Fig. 5, we find that:

(1) For low-dimensional system A, there exists a reentrant behavior in the phase diagram.

(2) For system B, the Néel temperature tends to zero as decreasing Δ .

(3) For higher-dimensional system C, there exists finite temperature phase transition in the isotropic Heisenberg limit $\Delta = 0$. Above studies are in accordance with the previous quantum Monte Carlo[15, 20, 39, 40] and mean field renormalization group[10, 11, 17, 41] results. From our results, we can see that as the value of d_f increases the phase transition will present in the isotropic Heisenberg limit and as the value of d_f decreases the reentrant behavior will appear, and $d_f = 2$ maybe the critical dimension. We consider this phenomena may are suitable for different fractal dimensions that is related to the quantum effects which will be discussed in Sec. V. Moreover, we also study the critical temperature when $\Delta \rightarrow 0$ and obtain the following law for system B (Fig. 6):

$$T_N \sim \frac{1}{\ln \Delta}. \quad (19)$$

IV. THE QUANTUM CORRELATIONS FOR THE THREE LATTICES

In this section, we study the QD between two non-nearest-neighbor end spins of AF Heisenberg model in three DH lattices at finite temperature and discuss the relations of QD with temperature and anisotropic parameter. It is widely accepted that quantum mutual information is a measure of the total correlation contained in a composite quantum system which includes classical and quantum correlations[42, 43]. We want to get quantum correlation by subtracting classical correlation from quantum mutual information. As a common representation of quantum correlation, QD captures nonclassical correlation even without entanglement. For a quantum state ρ_{12} of the composite system containing subsystems 1 and 2, the QD is defined as

$$D(\rho_{12}) = I(\rho_{12}) - C(\rho_{12}),$$

where $I(\rho_{12})$ is the quantum mutual information and $C(\rho_{12})$ is the classical correlation[28, 44]. Because the density matrix ρ_{12} of two spins in AF Heisenberg model exhibits an X

structure, it is called X state, as

$$\rho_{12} = \begin{pmatrix} a_{11} & 0 & 0 & a_{14} \\ 0 & a_{22} & a_{23} & 0 \\ 0 & a_{32} & a_{33} & 0 \\ a_{41} & 0 & 0 & a_{44} \end{pmatrix},$$

where

$$\begin{aligned} a_{11} &= a_{44} = \frac{e^K}{2e^K + e^K + e^{K(1-2\Delta)}}, \\ a_{14} &= a_{41} = 0, \\ a_{22} &= a_{33} = \frac{e^{K(1-2\Delta)} + e^{K(2\Delta-3)}}{2(2e^K + e^{K(2\Delta-3)} + e^{K(1-2\Delta)}),} \\ a_{23} &= a_{32} = \frac{e^{K(1-2\Delta)} - e^{K(2\Delta-3)}}{2(2e^K + e^{K(2\Delta-3)} + e^{K(1-2\Delta)}).} \end{aligned}$$

For two-qubit X state, there are some effective numerical and analytical expressions[44–46]. In this manuscript, we adopt the method in the Refs.[44, 47] to obtain the QD of the two sites, we don't give the analytical expression here, because the form is complicated. Then the numerical result of QD is obtained between two end sites on the fractal lattices by implementing the decimation RG method[48–50].

Fig. 7 shows the QD varies the temperature T (with the unit $|J|/k_B$) and anisotropy parameter Δ in system A containing L sites. The variation of the QD between two end spins with temperature T is shown in Figs. 7(a) and (b). It can be seen that the QD exists maximum at $T = 0$ and decreases with the increase of $k_B T/|J|$; the QD decreases with the increase of L , and it is almost zero when $L \geq 30$. From Figs. 7(c) and (d) we can find that the QD decreases with the increasing Δ , no matter how large the size of system is, QD will change to 0 in the Ising limit $\Delta = 1$ and there is a turning point in the isotropic Heisenberg limit $\Delta = 0$. Fig. 8 shows a continuous change of QD with T and Δ . We can find that in case of $L = 2$, there is a certain mutation in the contour of QD at $\Delta = 0$; In case of $L > 2$, there exists the "cusp" of the contour at $\Delta = 0$.

Figs. 9 and 10 show the QDs vary the temperature T and anisotropy parameter Δ in systems B and C. Their basic rule is similar to system A, but QDs still exist when the size of system is large ($L = 2732$ and $L = 779$ correspond to systems B and C, respectively). And we find that when $T \rightarrow 0$, there is a great difference of QD on both sides of $\Delta = 0$ by the calculation results. When $\Delta > 0$ and $T \rightarrow 0$, the QD is reduced in turn with the

increase of L until $L \geq 684$, there exists almost no QD; When $\Delta \leq 0$ and $T \rightarrow 0$, the QD of $L > 2$ exists a fixed value, which is shown in Figs. 9(a) and (b). From Figs. 9(c) and (d), we can find that there are a turning point of QD for all case at $\Delta = 0$. When $\Delta > 0$ and $\Delta < 0$, the system tends to be the Ising model and XY model, respectively. As shown in Fig. 10, in system C not only there is a turning point but also there is a cross point of the QD at $\Delta = 0$, the turning degree gradually increases with the increase of L . In order to further study the relation of QD with T and Δ , we prepare the contour plots of QD of systems B (Fig. 11) and C (Fig. 12), which show a continuous change of QD with Δ and T . We can find that in case of $L = 2$, there is a certain mutation in the contour at $\Delta = 0$; In case of $L > 2$, there exists the cusp of the contour at $\Delta = 0$.

V. THE QUANTUM EFFECT

In this section, we discuss the effect of quantum fluctuation and analyze the error of result which is induced by the noncommutativity. We note that, we can deal with a classical system straightforwardly, because there will be no noncommutative. However, for quantum systems, it can not be solved by such simplifying process because of the noncommutativity between the Hamiltonians of the neighboring generators[51]. In the following, we take system A as an example to discuss this effect which is the discrepancy existing between the exact result and the approximate one. Firstly, we assume the generator of system A (Fig. 2(a1)) as the whole system that we will calculate. In this case, noncommutative is neglected and the rigorous result can be obtained as $(K'(K, \Delta), \Delta'(K, \Delta))$. For the same system, we apply the Migdal-Kadanoff method and obtain the approximative result which is defined as $(2K''(K, \Delta; K, \Delta; K, \Delta), \Delta''(K, \Delta; K, \Delta; K, \Delta))$. Finally, using the convenient ratios proposed in Ref. [37], we define the errors as

$$E^K \equiv \frac{2K''(K, \Delta; K, \Delta; K, \Delta)}{K'(K, \Delta)} - 1, \quad (20)$$

$$E^\Delta \equiv \frac{\Delta''(K, \Delta; K, \Delta; K, \Delta)}{\Delta'(K, \Delta)} - 1. \quad (21)$$

The T -dependence of E_F^K , E_F^Δ (for the ferromagnetic case) and E_{AF}^K , E_{AF}^Δ (for the AF case) for typical values of Δ is presented in Fig. 13. As we can see, both E^K and E^Δ tend to zero in the $T \rightarrow \infty$, and in the Ising limit ($\Delta = 1$), both E^K and E^Δ equal zero at all temperature which is in accordance with the previous conclusion [52]. In the range of low temperature,

the quantum effect of the AF system is stronger than that of the ferromagnetic system. With the decrease of Δ , the effect of the fluctuation will be strengthened for both ferromagnetic and AF systems. The ordering is destroyed by the quantum fluctuation and this fact is responsible for the reentrant behavior in the phase diagram of system A. Furthermore, the competition between the quantum fluctuation and the thermal one is very important. At finite temperature, quantum fluctuation is usually suppressed in comparison with thermal one. However, when the temperature is close to zero, the quantum fluctuation dominate the critical behavior of the system. For systems B and C, we analyze the phase diagrams and consider that when the Néel temperature is relatively high, i.e., the thermal fluctuation is dominated, the ordering will not be destroyed and there exists phase transition when Δ is close to zero.

VI. SUMMARY

We have investigated the phase diagrams, critical phenomena and QDs of the spin-1/2 AF Heisenberg model on the DH systems A, B and C. For system A, we have found the reentrant behavior in the critical line and our results also show that $T_N \sim \frac{1}{\ln(\Delta_c - \Delta)}$ when T is close to zero. Moreover, it is found that the Néel temperature of system B tends to zero and there exists finite temperature phase transition in system C. We have also found that no matter how large the size of system is, QD will change to zero in the Ising limit and there is a turning point of QD in the isotropic Heisenberg limit $\Delta = 0$ where there is a "peak" of the contour for the systems studied. And the QD decreases with the increase of L , and it is almost zero in system A when $L \geq 30$. For system B and C, the QDs still exist when the size of system is larger than that of system A. In the end, taking system A as an example, the error of result is analyzed and our result indicate that quantum fluctuation is the cause of the reentrant behavior in the phase diagram.

Acknowledgments

This work is supported by the National Natural Science Foundation of China under Grants No. 11675090 and No. 11905095; the Shandong Natural Science Foundation under Grant No. ZR2020MA092. P.-P. Zhang would like to thank Zhong-Qiang Liu, Yue Li,

Zhen-Hui Sun, Li-Zhen Hu and Jing Wang for fruitful discussions and useful comments.

- [1] Z. R. Yang, Fractal physics. Shanghai Scientific and Technological Education Publishing House, Shanghai (1996).
- [2] S. N. Kempkes, M. R. Slot, S. E. Freney, S. J. M. Zevenhuizen, D. Vanmaekelbergh, I. Swart and C. Morais Smith, Nat. Phys. **15**, 127 (2018).
- [3] Y. Gefen, B. B. Mandelbrot, A. Aharony, Phys. Rev. Lett. **45**, 855 (1980).
- [4] Y. Gefen, A. Aharony, B. B. Mandelbrot, J. Phys. A: Math. Gen. **16**, 1267 (1983).
- [5] J. A. Plascak, J. Phys. A: Math. Gen. **17**, L597 (1984).
- [6] J. Ricardo de Sousa, N. S. Branco, B. Boechat, C. Cordeiro, Physica A **328**, 167 (2003).
- [7] A. M. Mariz, R. M. Zorzenon dos santos, C. Tsallis and R. R. dos santos, Phys. Lett. **108A**, 95 (1985).
- [8] R. Chitra, S. Pati, H. R. Krishnamurthy, D. Sen, and S. Ramasesha, Phys. Rev. B **52**, 6581 (1995).
- [9] N. S. Branco and J. Ricardo de Sousa, Phys. Rev. B **62**, 5742 (2000).
- [10] J. Ricardo de Sousa, and I. G. Araujo, Phys. Lett. A **272**, 333 (2000).
- [11] I. G. Araujo, J. Ricardo de Sousa, and N. S. Branco, Physica A **305**, 585 (2002).
- [12] P. J. Jensen, K. H. Bennemann, D. K. Morr and H. Dreyssé, Phys. Rev. B **73**, 144405 (2006).
- [13] R. P. Singh, Z. C. Tao, and M. Singh, Phys. Rev. B **46**, 1244 (1992).
- [14] C. M. Soukoulis, S. Datta, and Y. H. Lee, Phys. Rev. B **44**, 446 (1991).
- [15] A. Cuccoli, T. Roscilde, V. Tognetti, R. Vaia and P. Verrucchi, Phys. Rev. B **67**, 104414 (2003).
- [16] T. Krokhmalkii, V. Baliha, O. Derzhko, J. Schulenburg, and J. Richter, Phys. Rev. B **95**, 094419 (2017).
- [17] J. Ricardo de Sousa and J. A. Plascak, Phys. Lett. A **237**, 66 (1997).
- [18] J. Ricardo de Sousa and I. G. Araújo, Solid State Commun. **115**, 265 (2000).
- [19] B. G. Liu, Phys. Rev. B **41**, 9563 (1990).
- [20] T. Roscilde, A. Cuccoli, and P. Verrucchi, physica status solidi (b) **236**, 433 (2003).
- [21] C. H. Bennett, G. Brassard, C. Crépeau, R. Jozsa, A. Peres, and W. K. Wootters, Phys. Rev. Lett. **70**, 1895 (1993).

- [22] A. Niezgoda, M. Panfil, and J. Chwedeńczuk, *Phys. Rev. A* **102**, 042206 (2020).
- [23] A. Szasz, *Phys. Rev. A* **99**, 062313 (2019).
- [24] S. Siwiak-Jaszek, T. P. Le, and A. Olaya-Castro, *Phys. Rev. A* **102**, 032414 (2020).
- [25] H. Ollivier and W. H. Zurek, *Phys. Rev. Lett.* **88**, 017901 (2001).
- [26] L. Henderson and V. Vedral, *J. Phys. A: Math. Gen.* **34**, 6899 (2001).
- [27] K. Modi, A. Brodutch, H. Cable, T. Paterek, and V. Vedral, *Rev. Mod. Phys.* **84**, 1655 (2012).
- [28] Y. L. Xu, X. Zhang, Z. Q. Liu, X. M. Kong, and T. Qi, *Ren Eur. Phys. J. B* **87**, 132 (2014).
- [29] G. Adesso, T. R. Bromley, and M. Cianciaruso, *J. Phys. A: Math. Theor.* **49**, 473001 (2016).
- [30] Y. CH. Huang, *Phys. Rev. B* **89**, 054410 (2014).
- [31] F. G. S. L. Brandão, M. Piani, and P. Horodecki, *Nat. Commun.* **6**, 7908 (2015).
- [32] V. Madhok and A. Datta, *Int. J. Mod. Phys. B* **27**, 1345041 (2013).
- [33] D. Girolami, A. M. Souza, V. Giovannetti, T. Tufarelli, J. G. Filgueiras, R. S. Sarthour, D. O. Soares-Pinto, I. S. Oliveira, and G. Adesso, *Phys. Rev. Lett.* **112**, 210401 (2014).
- [34] K. Brádler, M. M. Wilde, S. Vinjanampathy, D. B. Uskov, *Phys. Rev. A* **82**, 062310 (2010).
- [35] M. Usman, K. Khan, *The European Physical Journal D* **74**, 181 (2020).
- [36] A. O. Caride, C. Tsallis, and S. I. Zanette, *Phys. Rev. Lett.* **51**, 145 (1983).
- [37] A. M. Mariz, C. Tsallis, and A. O. Caride, *J. Phys. C* **18**, 4189 (1985).
- [38] Y. Qin, and Z. R. Yang, *Phys. Rev. B* **43**, 8576 (1991).
- [39] S. S. Aplesnin, *J. Phys: Condens. Mat.* **10**, 10061 (1998).
- [40] W. G. Clark and L. C. Tippie, *Phys. Rev. B* **20**, 2914 (1979).
- [41] J. Ricardo de Sousa, *Phys. Lett. A* **216**, 321 (1996).
- [42] B. Groisman, S. Popescu, and A. Winter, *Phys. Rev. A* **72**, 032317 (2005).
- [43] B. Schumacher and M. D. Westmoreland, *Phys. Rev. A* **74**, 042305 (2006).
- [44] M. Ali, A. R. P. Rau, and G. Alber, *Phys. Rev. A* **81**, 042105 (2010).
- [45] J. Maziero, T. Werlang, F. F. Fanchini, L. C. Céleri, R.M. Serra, *Phys. Rev. A* **81**, 022116 (2010).
- [46] Q. Chen, C. Zhang, S. Yu, X. X. Yi, C. H. Oh, *Phys. Rev. A* **84**, 042313 (2011).
- [47] Y. CH. Huang, *Phys. Rev. B* **88**, 014302 (2013).
- [48] A. N. Berker, S. Ostlund, *J. Phys.: Condens. Matter* **12**, 4961 (1979).
- [49] R. B. Griffiths, M. Kaufman, *Phys. Rev. B* **26**, 5022 (1982).
- [50] M. Kaufman, R.B. Griffiths, *Phys. Rev. B* **30**, 244 (1984).

[51] H. Takano and M. Suzuki, J. Stat. Phys **26**, 635 (1981).

[52] J. Fröhlich and E. H. Lieb, Phys. Rev. Lett. **38**, 440 (1977).

Figure Captions

Fig. 1 The structure of three DH lattices. (a) The dimers. (b) The generators. (c) The generative lattices. They all start from the dimer and generate the lattices in an iterative manner.

Fig. 2 The procedure of RG transformation. (a) System A: using the real-space RG method straightforwardly. (b) System B: the first step from (b1) to (b2) is the equivalent transformation and the second step from (b2) to (b3) is the RG transformation.

Fig. 3 Phase diagram of the AF and ferromagnetic Heisenberg models of system A. The red line corresponds to the AF Heisenberg case and the inset shows the phase diagram of ferromagnetic case. O(D) stands for ordered (disordered) phase. The open circle and the full square denote the unstable and fully stable fixed points, respectively.

Fig. 4 The scaling behaviors of system A when $T \rightarrow 0$. (a) and (b) represent the critical temperature T_c of ferromagnetic case and the Néel temperature T_N of AF case vary with Δ , respectively.

Fig. 5 Phase diagrams of the three systems. There exists a reentrant behavior in system A, the Néel temperature tends to zero as decreasing Δ in system B and there exists finite temperature phase transition in the isotropic Heisenberg limit $\Delta = 0$ in system C.

Fig. 6 The scaling behavior of system B in the $\Delta \rightarrow 0$ limit. The Néel temperature T_N is inversely proportional to $\ln \Delta$.

Fig. 7 The QD between two end spins on system A with L sites varies with T (with the unit $|J|/k_B$, the same below) and anisotropy parameter Δ . (a) and (b) the QD varies with T , (c) and (d) the QD varies with Δ . The QD for different L cases has a turning point at $\Delta = 0$.

Fig. 8 The contour plot of QD of system A with L sites varies with T and Δ . When $L = 2$, there is a certain mutation in the contour of QD at $\Delta = 0$; When $L > 2$, there exists the "cusp" in the contour of QD at $\Delta = 0$.

Fig. 9 The QD between two end spins of system B with L sites varies with with T and Δ . (a) and (b) the QD varies with T , (c) and (d) the QD varies with Δ . The QD for different L cases has a turning point at $\Delta = 0$.

Fig. 10 The QD of system C varies with T and Δ . (a) and (b) the QD varies with T , (c) and (d) the QD varies with Δ . The QD for different L cases has a cross point and a turning point at $\Delta = 0$.

Fig. 11 The contour plot of system B with L sites varies with T and Δ . When $L = 2$, there are a mutation in the contour of QD at $\Delta = 0$; When $L > 2$, there exists the "cusp" in the contour of QD at $\Delta = 0$.

Fig. 12 The contour plot of system C. When $L = 2$, there is a mutation in the contour of QD at $\Delta = 0$; When $L > 2$, there exists the "cusp" in the contour of QD at $\Delta = 0$.

Fig. 13 Thermal dependence of the errors E^K and E^Δ for the ferromagnetic and AF systems defined by Eq. (20) and Eq. (21), for typical values of Δ . (a) and (b) correspond to E^K , (c) and (d) correspond to E^Δ . It can be seen obviously that E^K and E^Δ for the ferromagnetic system are larger than the AF system at low temperature. Our calculations also show E^K and E^Δ equal zero in the Ising limit ($\Delta = 1$).

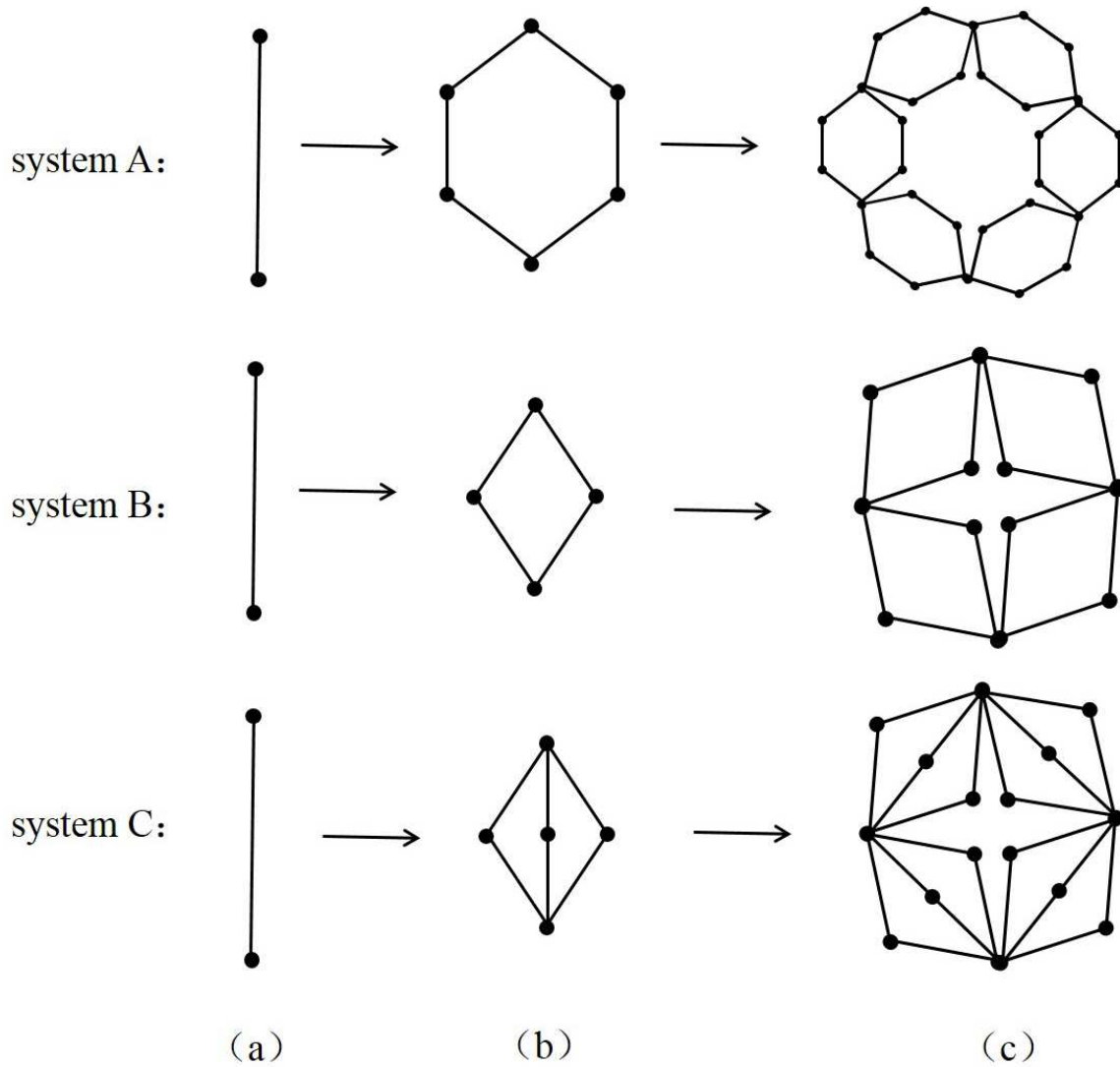


Fig. 1

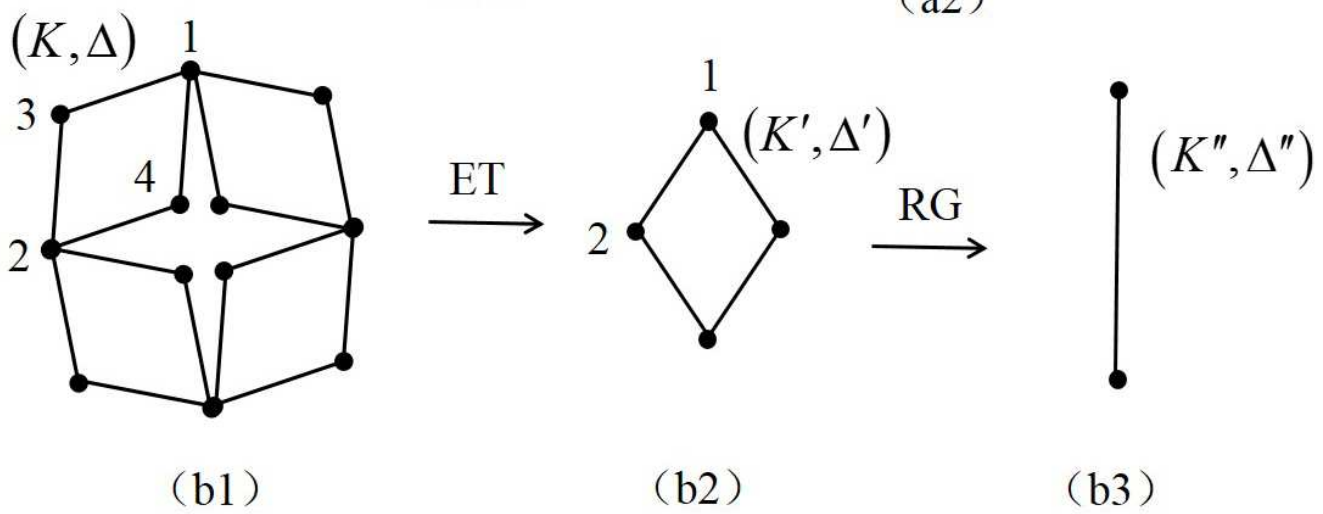
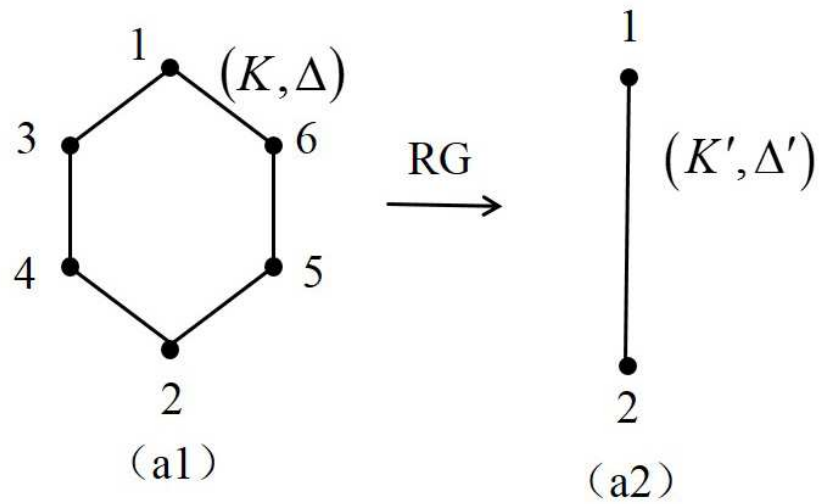


Fig. 2

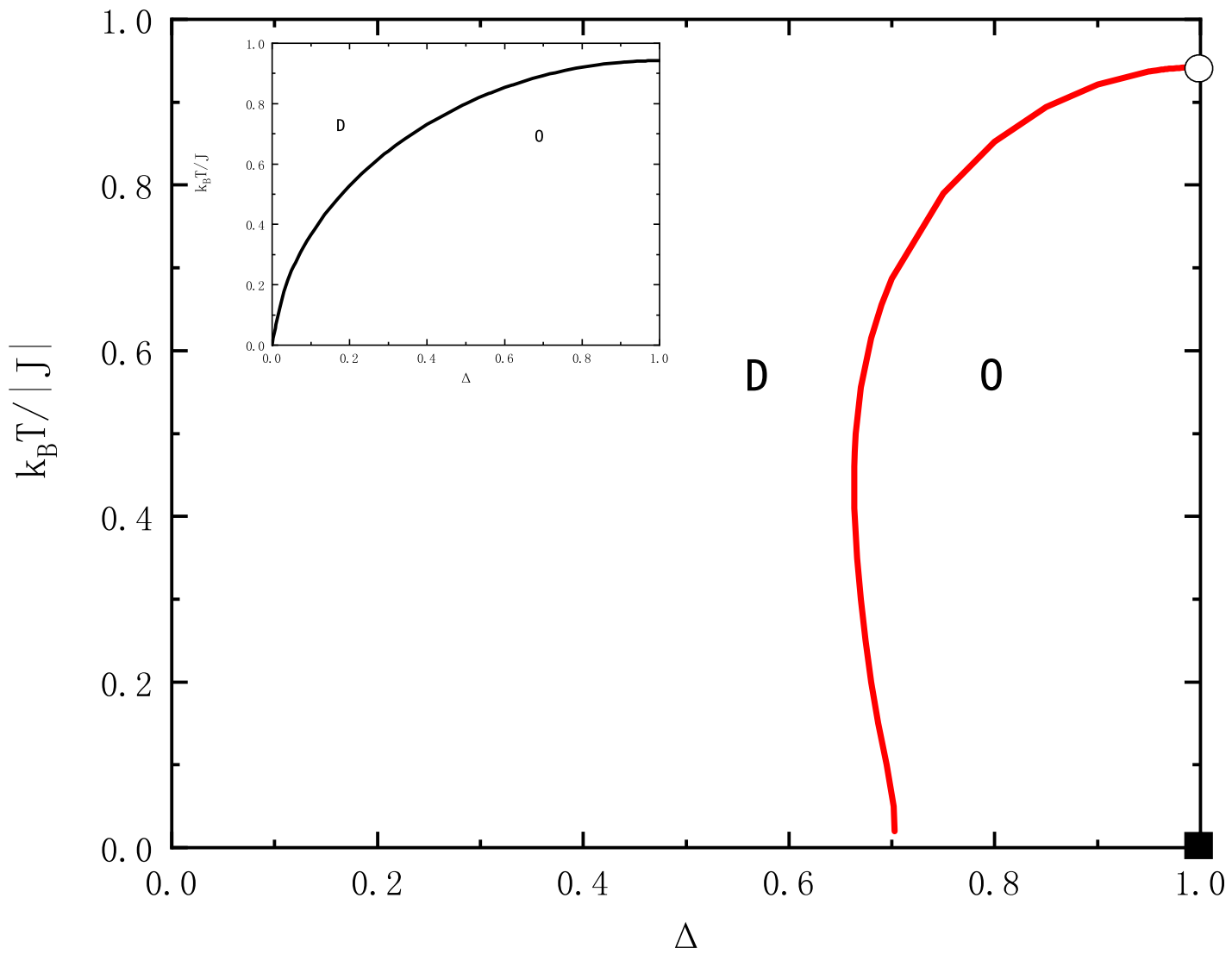


Fig. 3

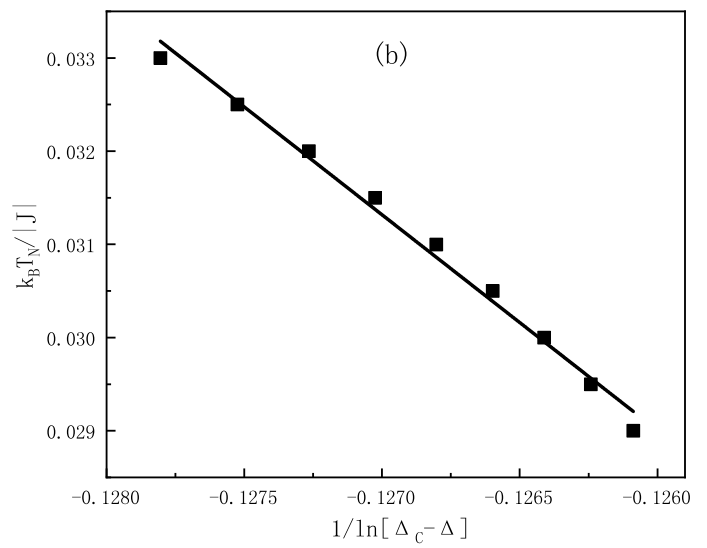
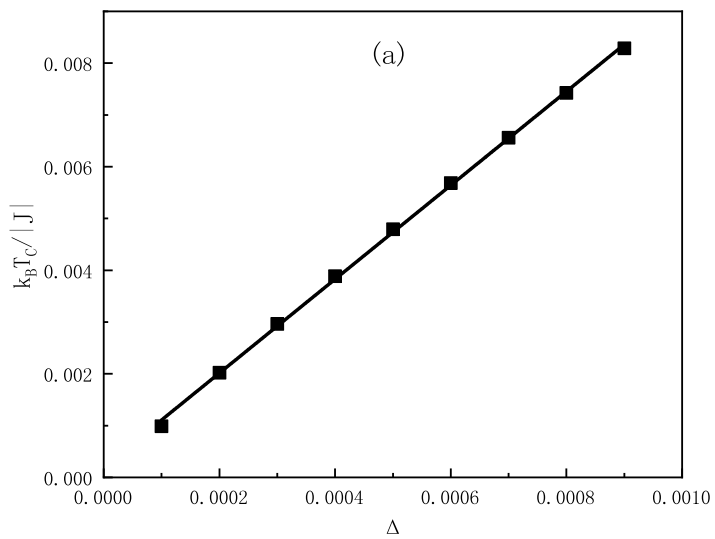


Fig. 4

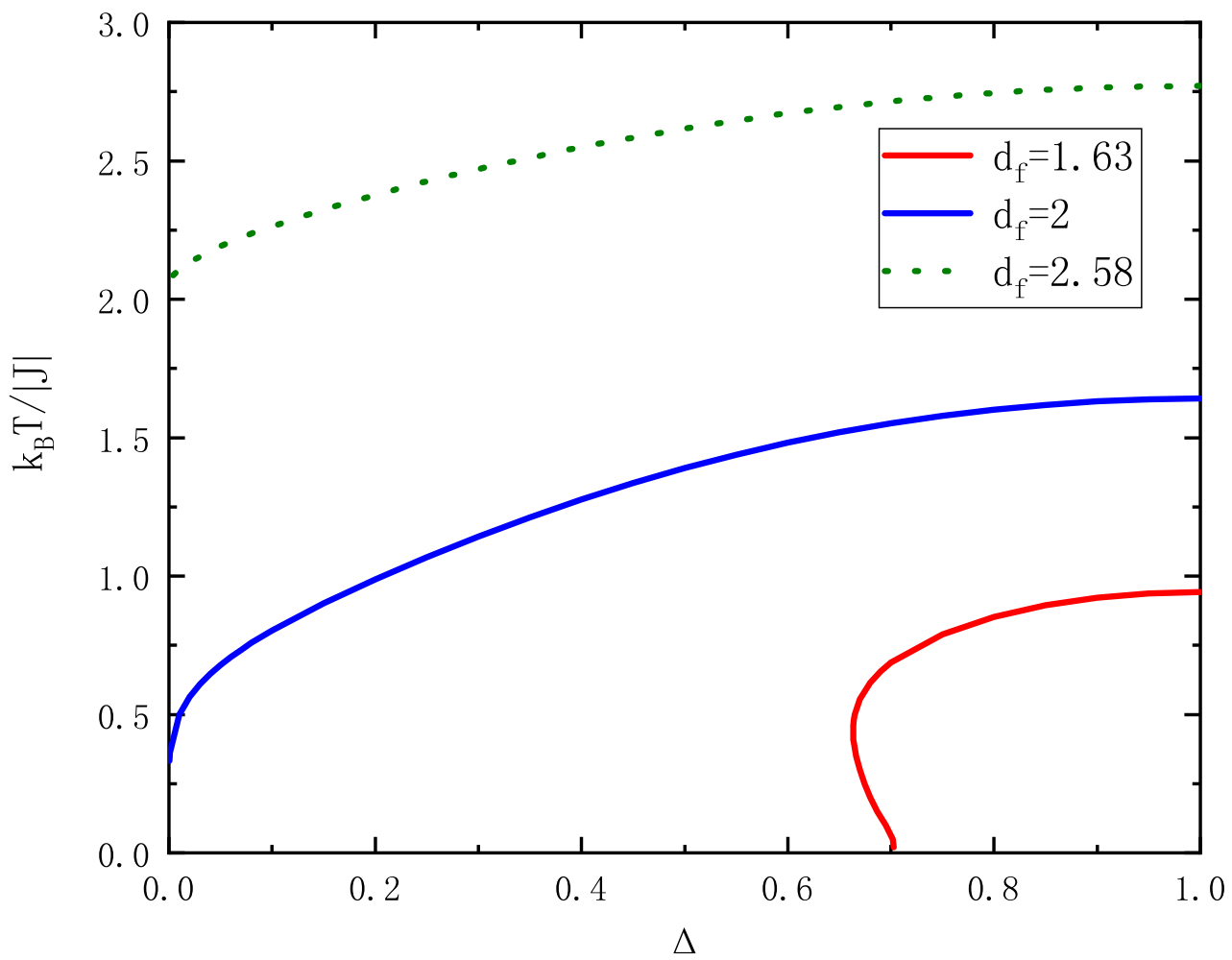


Fig. 5

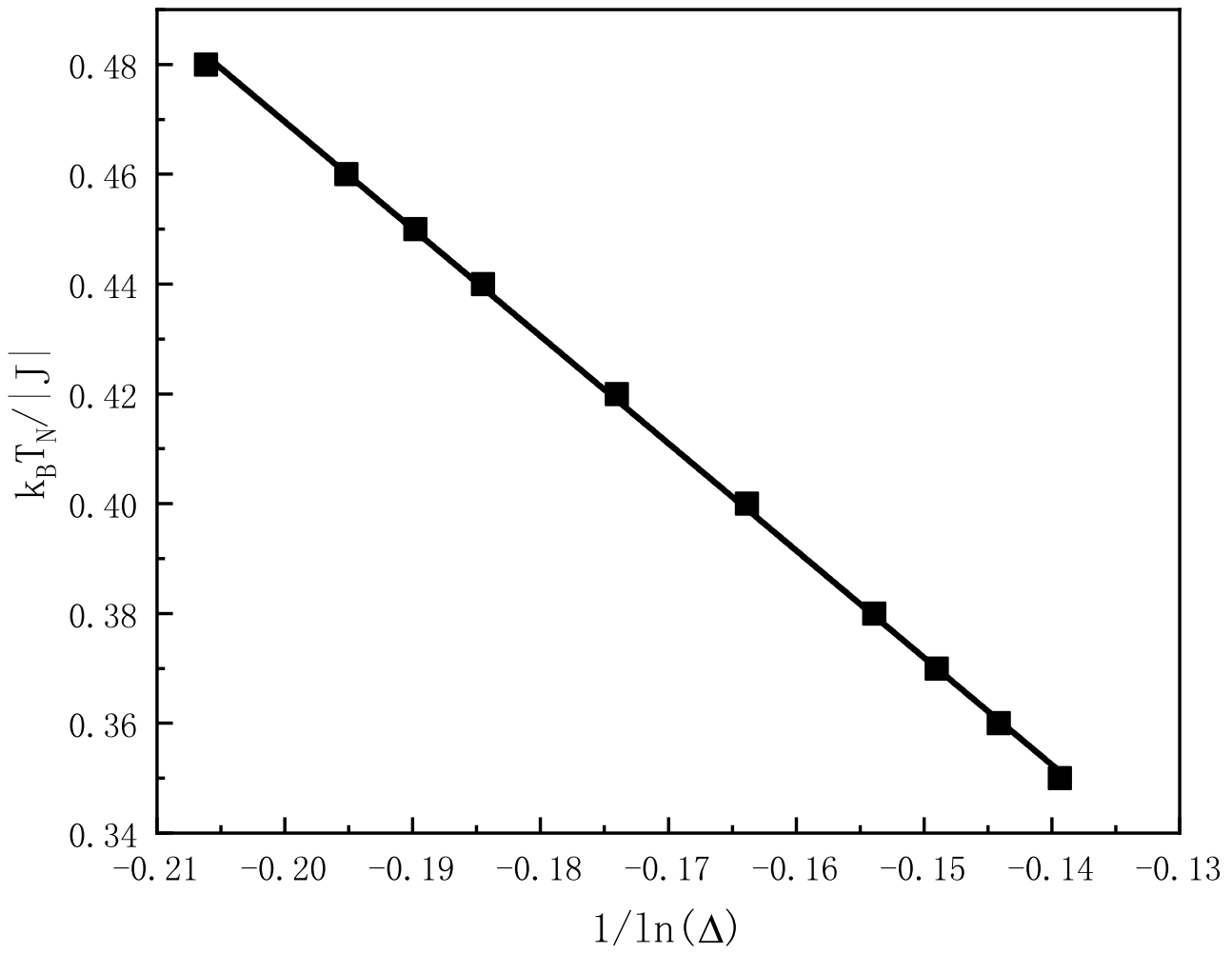


Fig. 6

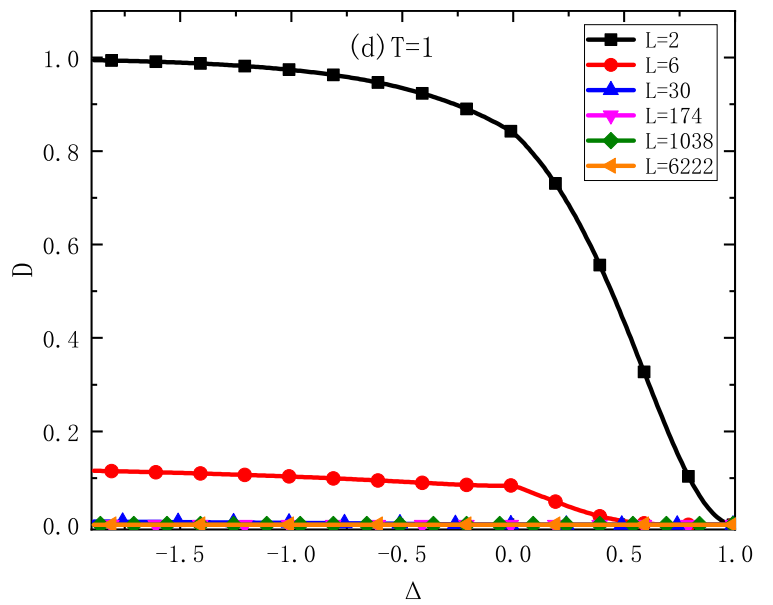
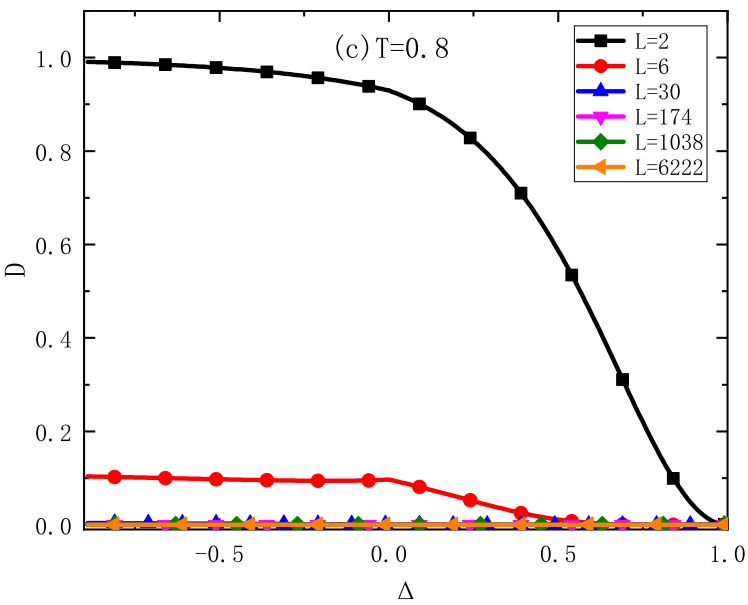
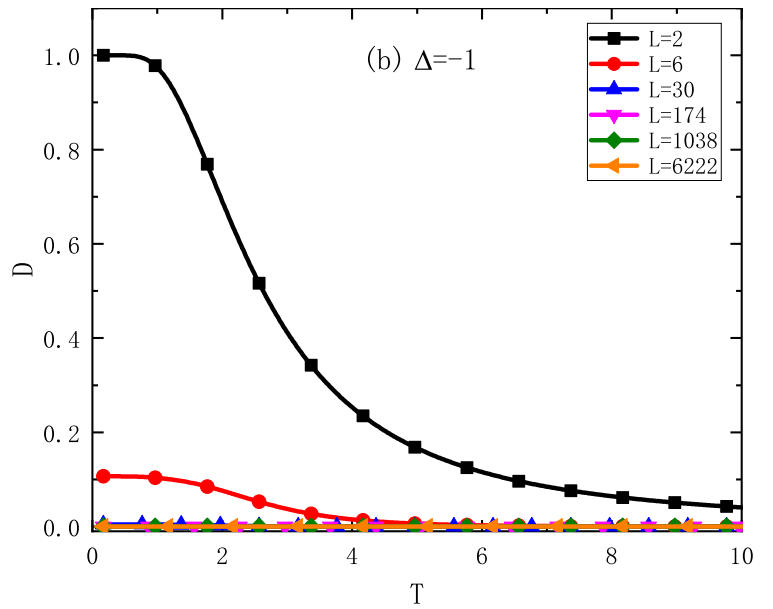
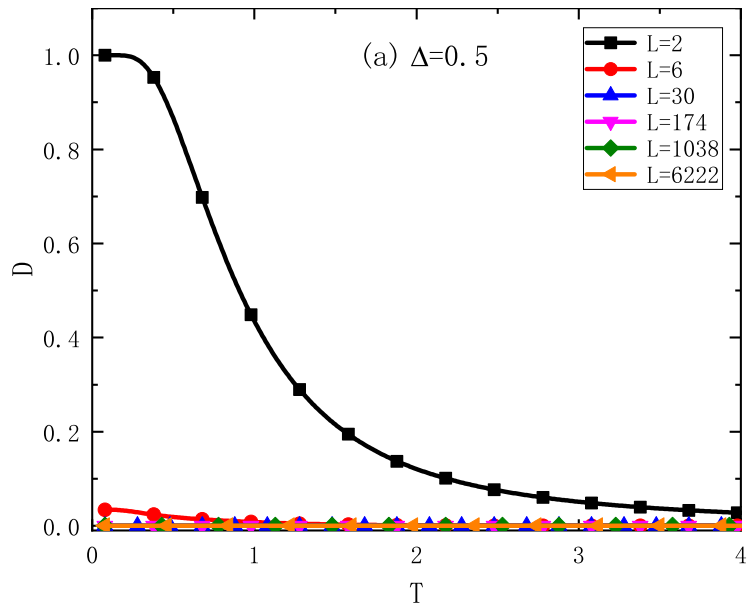


Fig. 7

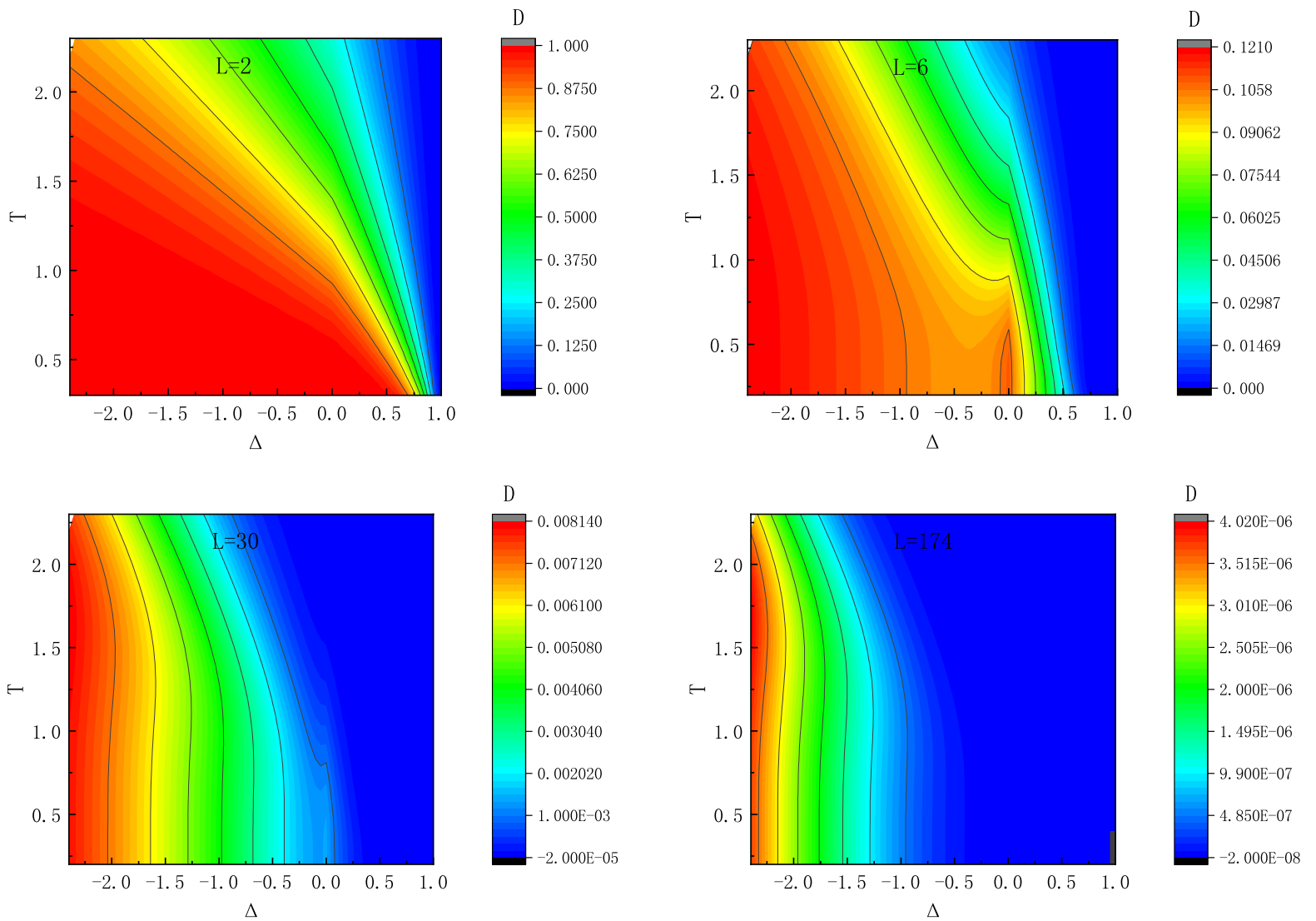


Fig. 8

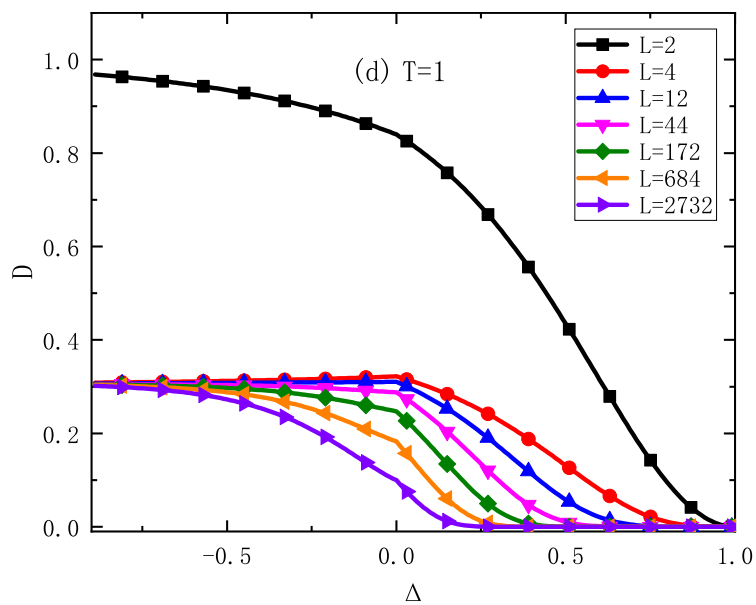
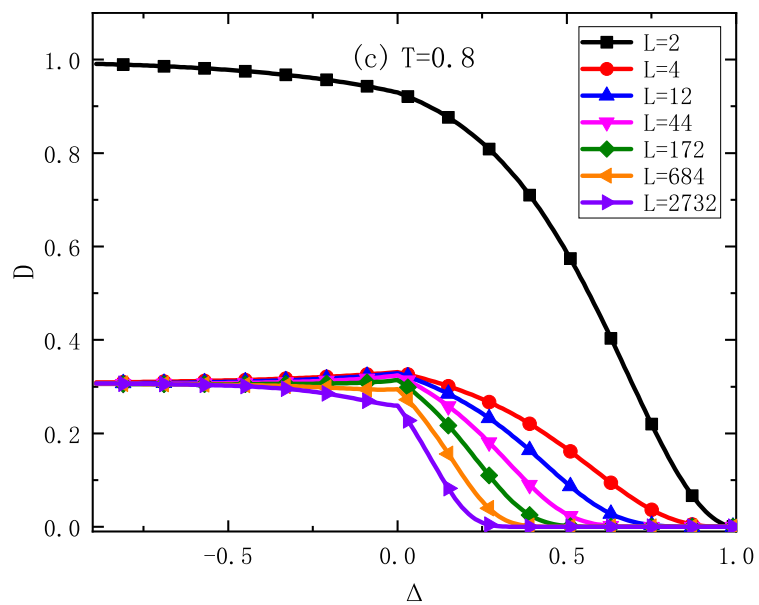
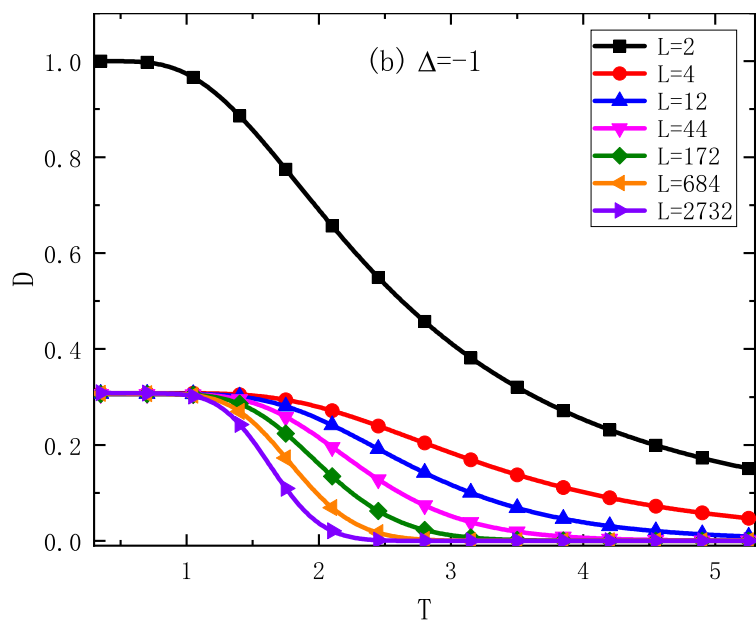
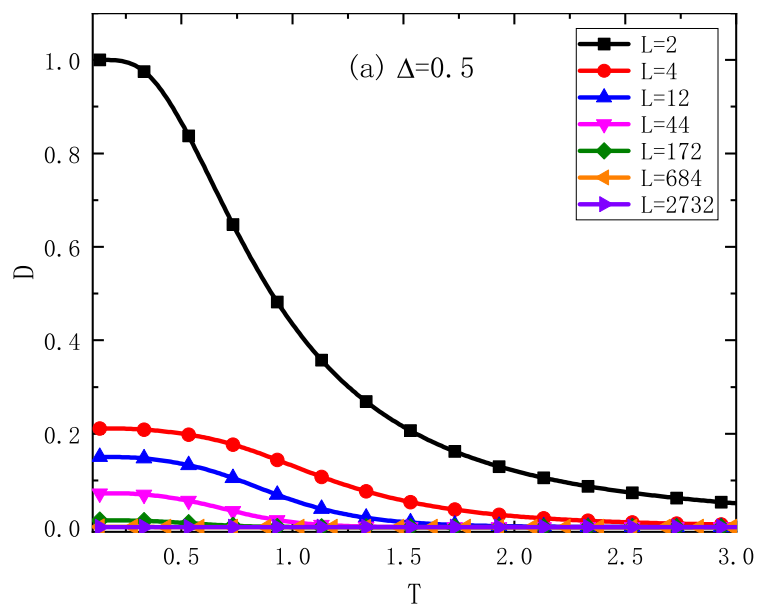


Fig. 9

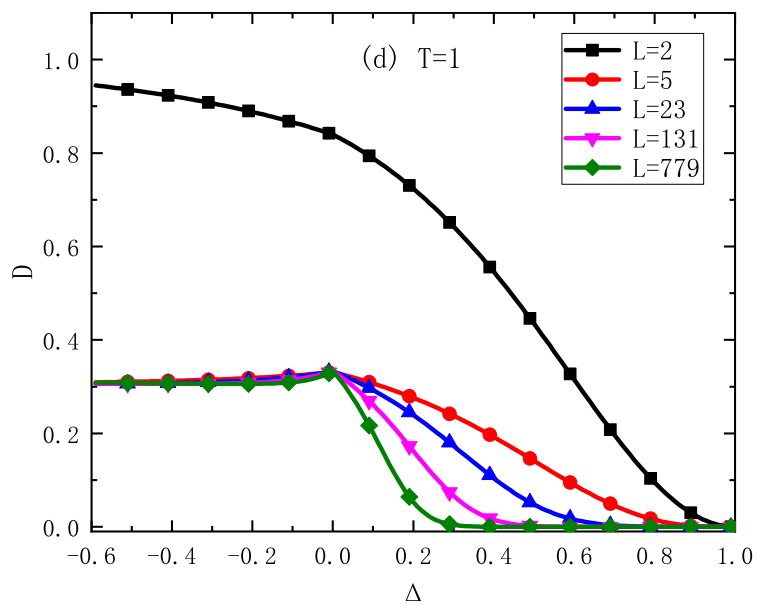
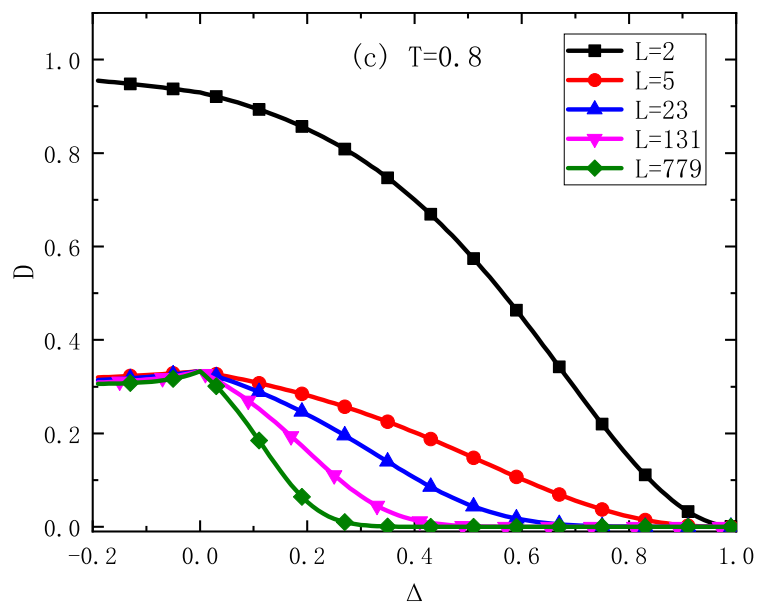
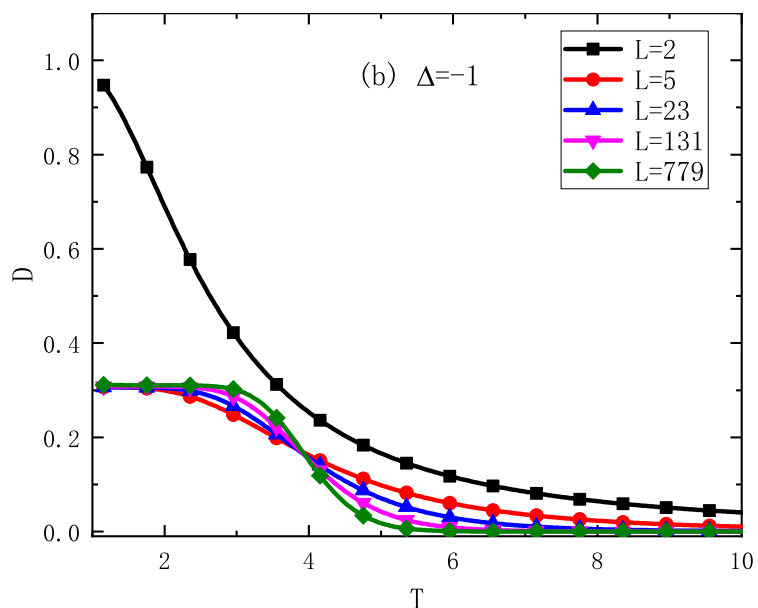
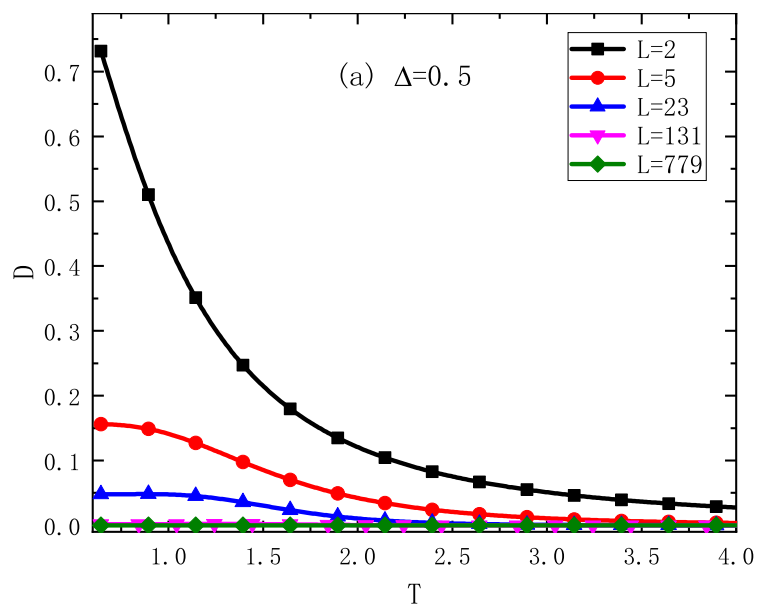


Fig. 10

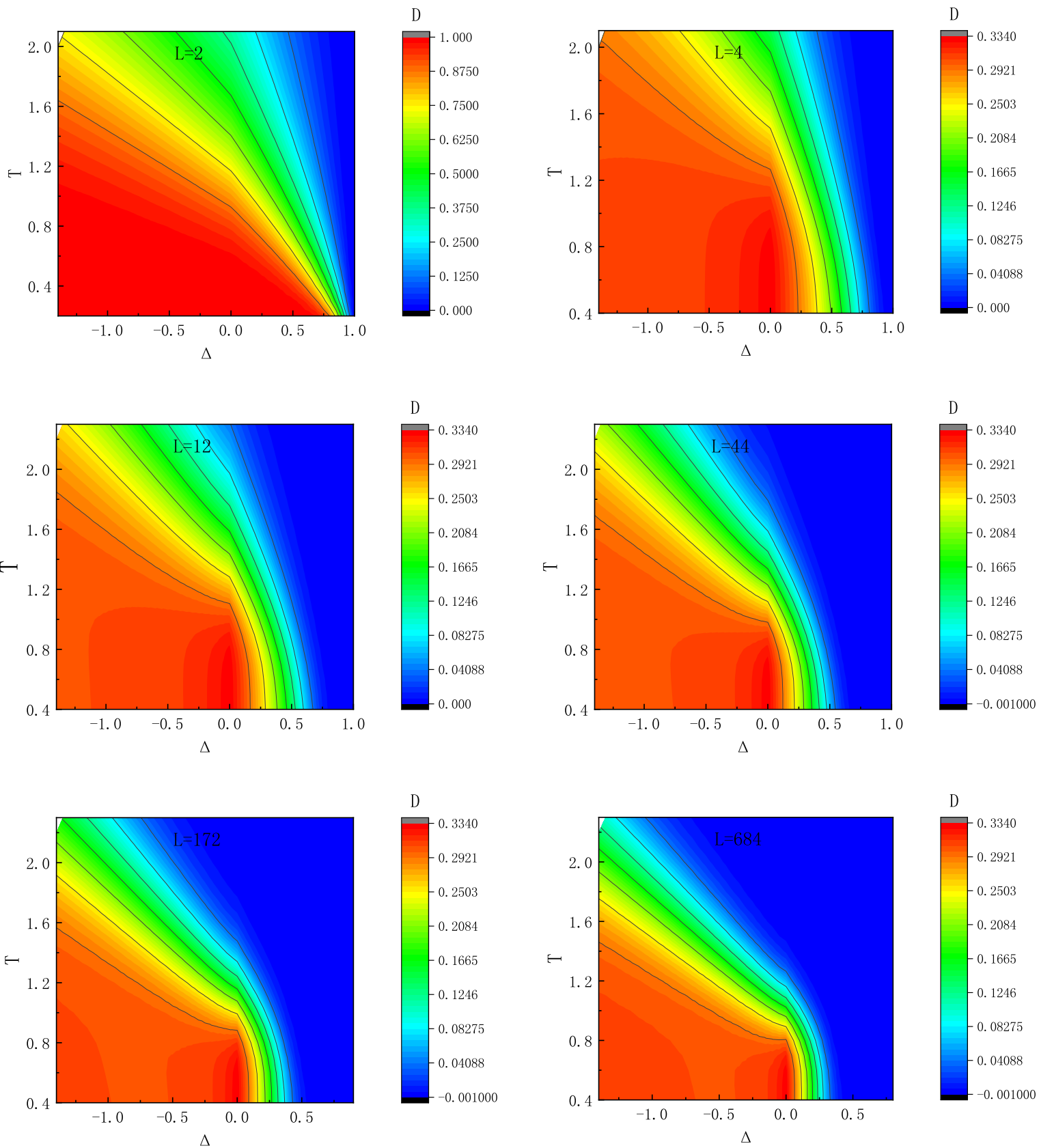


Fig. 11

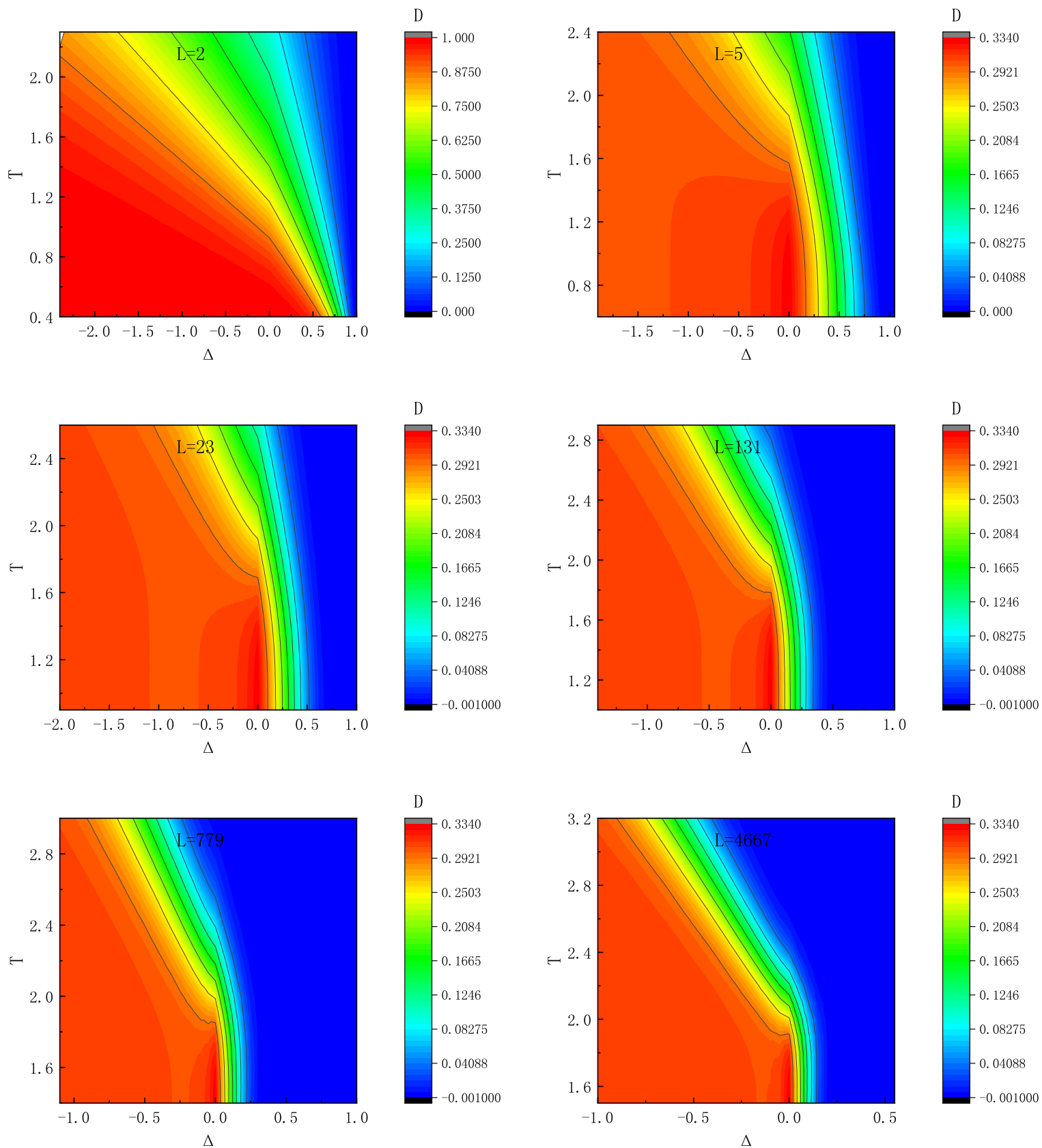


Fig. 12

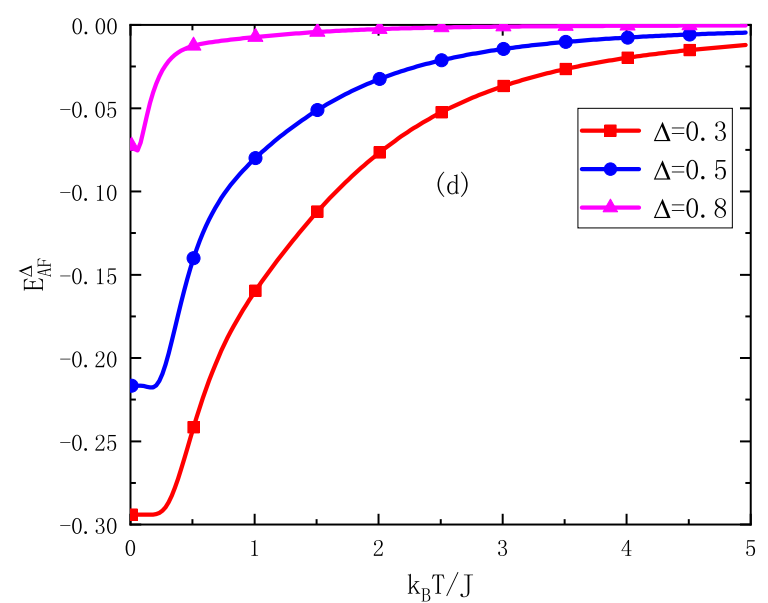
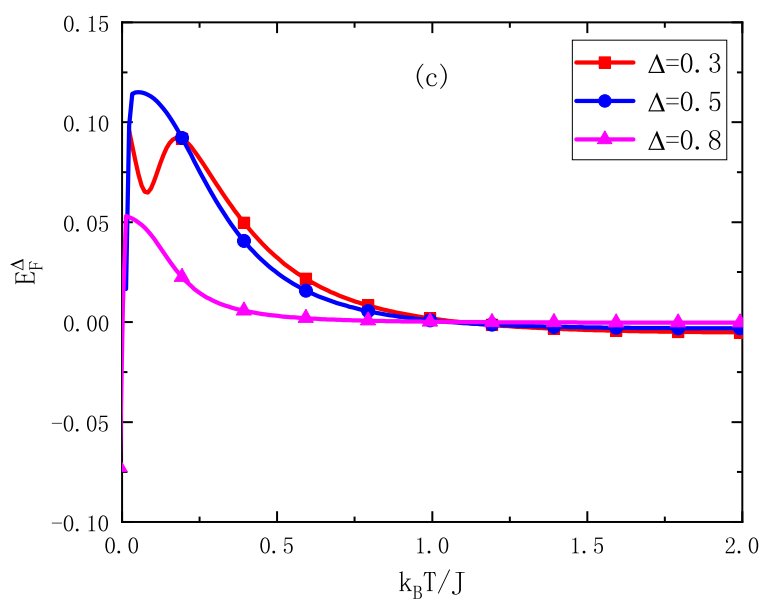
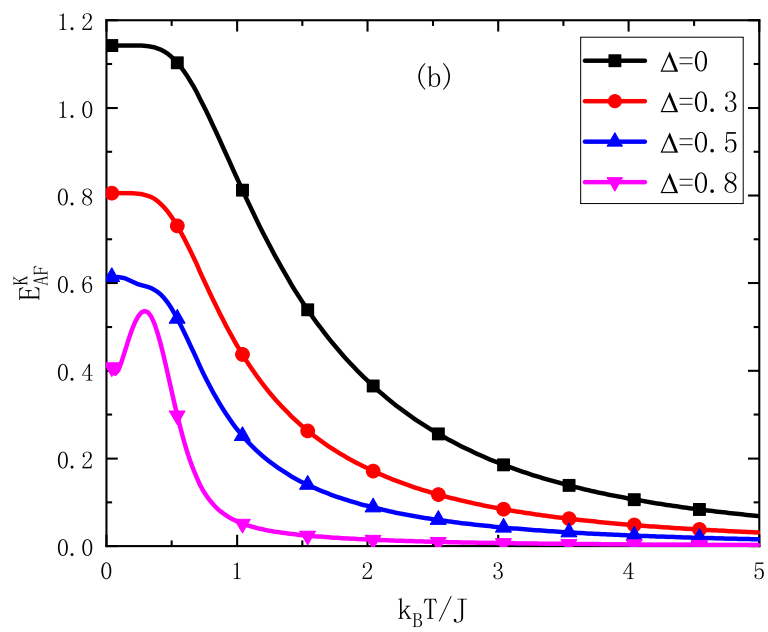
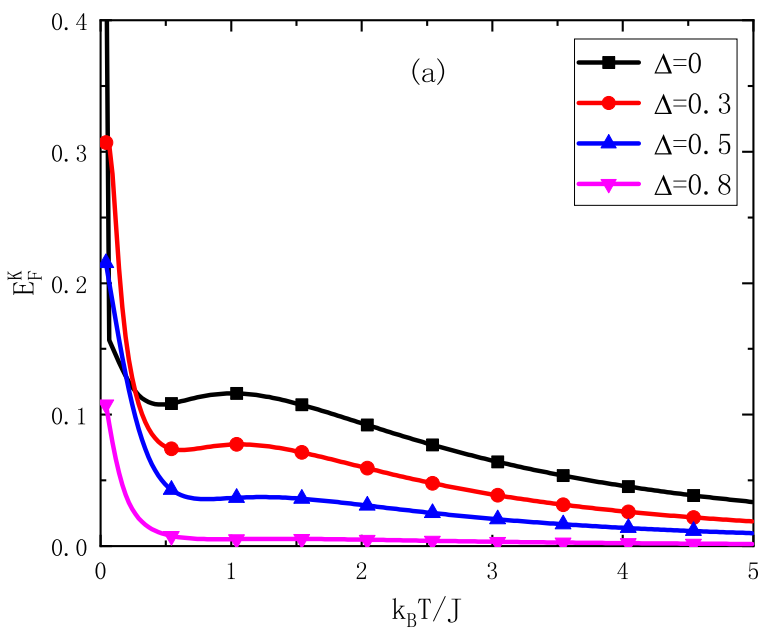


Fig. 13